Plasmonics (2015) 10:901–909
DOI 10.1007/s11468-015-9878-5

The Effects of Varying Dielectric Spacer Height on the Reflection Resonance Spectrum of Gold Nanorod-on-Mirror Grating Structure

Mehrdad Irannejad · Bo Cui · Mustafa Yavuz

Received: 24 September 2014 / Accepted: 4 January 2015 / Published online: 29 January 2015

Abstract Surface plasmon resonance properties of gold nanorod-on-mirror (with a dielectric spacer in between) grating structure were numerically investigated to obtain optimum geometrical parameters for achieving high reflection sensitivity and narrow resonance linewidth. It was found that the reflection resonance linewidth and intensity of the grating structures for different liquids depend on the nanorod height and the dielectric spacer height. However, there was no significant change in the reflection resonance position of the grating structures. The reflection resonant wavelength of the gold nanorod-on-mirror grating structure was increased by 22 nm on increasing refractive index by 0.044, which was accompanied by 1.3 nm reduction in the resonance linewidth. The maximum sensitivity in liquid was obtained as 529 nm/RIU in a grating structure with nanorod height of 25 nm at Δn=0.034. The minimum reflection resonance linewidth of 6 nm was reported for the first time. The proposed grating structure could be a promising candidate for sensing liquids whose refractive index is close to the water, including salinity and hemoglobin concentration measurement.

Keyword Surface plasmon · Localized surface plasmon · Hybrid mode · Reflection · Narrow linewidth · Sensor

Introduction

The surface plasmon behavior at the noble metal film and dielectric material interfaces has gained a broad interest in the last two decades [1–8]. Engineering of confined surface plasmon resonance at the interface of metallic nanostructure-dielectric material has potential applications in bio/chemical sensing [9–16] due to enhancement and confinement of electromagnetic field at the structural interfaces [17].

Surface plasmons, in general, is categorized as localized surface plasmon (LSP) and propagated surface plasmon (PSP) [17, 18]. The latter one, so-called surface plasmon polariton (SPP), is coupled with the incident electromagnetic field in the dielectric medium constructively and propagates as evanescent mode along the metal surface in a waveguide-like mode until it is completely absorbed at distance L (SPP propagation length) [17]. However, in the case of the localized surface plasmon, the incident electromagnetic field is absorbed/scattered by oscillating electrons of the electric dipole or quadrapole in the metallic nanoparticles [18]. The localized surface plasmon and propagated surface plasmon can also interfere constructively at the interfaces, producing hybrid modes [19], and its resonance wavelength is extremely sensitive to the refractive index of the surrounding dielectric materials [20–22].

Spatial distribution of electromagnetic field enhancement which is attributed to the interaction between LSP and SPP modes is another main factor that affects the characteristics of surface plasmon resonance spectra. This interaction could be acquired as LSP-LSP coupling between two adjacent nanostructures [23] and/or between LSP (of a nanostructure)-SPP (of metallic film surface) modes [12, 24].

The LSP-SPP interaction can be utilized in a metal nanoparticle on a metal film (NPOM) system that has received less attention. For example, when nanoparticles are placed in close vicinity (~50 nm or less) to the film surface, a complex new hybrid plasmon modes are formed which results in more electromagnetic enhancement at close vicinity of the structure [25–27]. These hybrid modes are mixture of LSP of the NPs

M. Irannejad (✉) · B. Cui · M. Yavuz
Waterloo Institute for Nanotechnology, University of Waterloo, Waterloo, ON, Canada
e-mail: mehrdad.irannejad@uwaterloo.ca

and SPP of the film, and their resonance properties have distinctive trends that depends on whether the LSP-SPP coupling or predominant LSP is used as excitation source [28].

It is also known that a surface electric dipole induces an image dipole in the substrate (i.e., conductor layer close to the dipole structure), and their interaction is enhanced if the incident electromagnetic field has perpendicular component to the substrate surface [29]. Recently, Mubeen et al. [12] studied the optical properties of randomly distributed gold NPOM system, where gold nanoparticles were separated from 200 nm thick gold film with different thickness of SiO_2, ZrO_2, and Al_2O_3. It was found that the measured resonance intensity using silica as spacer layer was higher than using Al_2O_3 and ZrO_2 at different thicknesses. However, by increasing the SiO_2 thickness from 2 to 10 nm, the surface plasmon resonance intensity was reduced significantly. Using ultrathin Al_2O_3 layer between the gold film and gold nanoparticles was also reported by Lumdee et al. [30], where the surface plasmon resonance wavelength was tuned in the range of 610 to 690 nm on reducing the oxide layer thickness from 3.2 to 0 nm. In another study, the large enhancement of electric field and high sensitivity of 648 nm/RIU followed by a Fano resonance with linewidth as small as 10 nm was achieved by placing asymmetric ring/disk plasmonic nanocavity on the optically thick gold film [24], which attributed to the induced image surface dipole and quadrapole in the gold film.

In this work, we will show that the performance of an Au nanorod-on-mirror (Au-NROM) grating structure depends strongly on the nanorod height and spacer height. Such structure can be used for detecting different type of liquids with refractive index in the range of 1.333 to 1.3777 with an unprecedented sensitivity of 500 nm/RIU and narrow reflection resonance linewidth as small as 7 nm without relying on the Fano resonance that is hard to control due to too narrow process window. For this purpose, a series of nanorods with different heights in the range of 25 to 75 nm and diameter of 200 nm were placed on the 100 nm thick gold film. The dielectric spacer (n=1.45) with different heights in the range of 10 to 50 nm was placed between the gold mirror film and gold nanorods, and water (n=1.333), Trimethylamine (n=1.45), acetone (n=1.356), human hemoglobin (n=1.367), and IPA (isopropanol alcohol, n=1.377) were considered as target liquids.

Methodology

Optical reflection spectrum of the incident electromagnetic field of the Au-NROM grating structure were numerically studied using the 3D full wavevector finite-difference time-domain (FDTD) method, which is the state-of-the-art method in solving Maxwell's equations in a complex geometries and dispersive media. FDTD is a discrete technique both in space and time, and Maxwell's equations are solved discretely in time and spatial grid of the so-called Yee cells [31]. The permittivity of gold nanorods and gold film were described by the Lorentz-Drude model and is given by [32, 33]

$$\varepsilon_\omega = \varepsilon_\infty + \sum_0^M \frac{f_m \omega_p^2}{\omega_m - \omega^2 + i\omega\Gamma_m} \tag{1}$$

where ε_∞ is the permittivity in the infinite frequency, ω and ω_p(=1.37188×10^{16} rad/s) are the incident and gold plasmon frequencies, respectively. The ω_m and Γ_m are the mth resonance and damping frequencies, respectively, which are obtained by fitting the empirical data of real and imaginary parts of the gold permittivity over a given wavelength region of interest.

For glass substrate and superstrate (i.e., target materials in sensing application) layers, the permittivity, $\varepsilon(\omega)$, values were assumed as n^2(=2.1025) and ${n_1}^2$, respectively, where n_1 is the refractive index of liquids. The FDTD was carried out using the commercial software package (FDTD Solution) from Lumerical Inc. The plane wave source, Au-NROM grating structure, and monitors were co-planar with boundary conditions that made them effectively infinite. In this study, an unpolarized plane wave of wavelength in the range of 400 to 900 nm with electric field amplitude of 1 V/m which propagates in the z-axis was used. The asymmetric and symmetric boundary conditions in the x-direction and the y-direction, respectively, and perfect matching layer (PML) in the z-direction were used to study the reflection properties at normal incidence of electromagnetic wave on the Au-NROM structure. The asymmetric and symmetric boundary conditions were considered instead of periodic boundary condition in order to reduce the calculation time [34]. The calculation grid resolution was as small as 2 nm (grid point-to-point distance) in the simulation cell, and combination of grading mesh and conformal meshing method which is offered by Lumerical FDTD package was used to calculate the electric and magnetic field at the corner and rounded region of the nanorods. This meshing method can allow to obtain accurate results for a given mesh size, even if the mesh size is twice as large, for example, 5 nm compared to 2.5 nm [34]. The calculation time was set as 350 fs, and the reflection spectra were calculated using an x-y monitor at 250 nm away from the nanorods/superstrate (liquid) interface. The plane wave source was placed 200 nm above the grating structure as shown in Fig. 1.

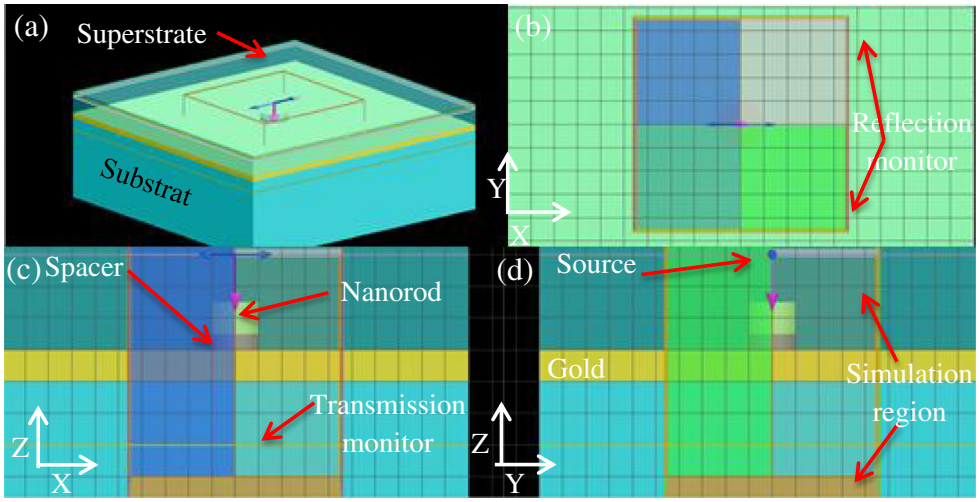

Fig. 1 The FDTD layout for Au-NROM grating in **a** perspective view, **b** XY view, **c** XZ view, and **d** YZ view

Results and Discussion

The Effects of Varying Structural Period

A series of numerical simulations were carried out to obtain the optimum value of the structural period in terms of maximum reflectinction (1-R, R is reflection) and narrow linewidth of resonance peak. In all simulations, the geometrical parameters of the Au-NROM were fixed as nanorod diameter of 200 nm, nanorod height of 25 nm, spacer (dielectric) height of 20 nm, and Au film thickness of 100 nm. The reflectinction profile of the Au-NROMs at water/grating structure interface, and different periods in the range of 400 to 1000 nm is shown in Fig. 2 and summarized in Table 1 for the hybrid mode.

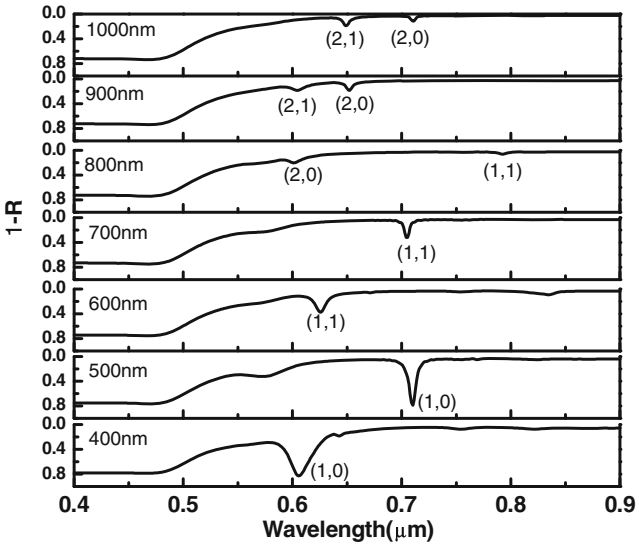

Fig. 2 FDTD calculated reflectinction spectrum at water/grating structure interface as a function of wavelength in the Au-NROM grating structure at different periods. The nanorod height, nanorod diameter, spacer height, film thickness, and ambient medium refractive index were fixed at 25 nm, 200 nm, 20 nm, 100 nm, and 1.333, respectively. The label (*i*,*j*) shows the surface plasmon resonance order at nanorod/spacer interface

The resonance peak of a square array at the metal/dielectric interface is given by [35]

$$\frac{2\pi}{\lambda_{\text{res}}}\sqrt{\frac{\varepsilon_m\varepsilon_d}{\varepsilon_m+\varepsilon_d}}=\frac{2\pi}{\lambda_{\text{res}}}\sin\theta+\left|\left(\pm i\ \overrightarrow{G_x}\pm j\overrightarrow{G_y}\right)\right| \tag{2}$$

where the ε_m and ε_d are the permittivity of the metal and dielectric medium, respectively. The λ_{res}, G_x, G_y, and θ are resonance wavelength, reciprocal lattice constant ($\frac{2\pi}{P}$) along the *x*- and *y*-axis for a square lattice and incident angle of electromagnetic field, respectively. The *i* and *j* are integers and *P* is the structural periodicity. For normal incidence electromagnetic field, θ=0, Eq. 2 reduces to

$$\lambda_{\text{res}}=\frac{P}{\sqrt{i^2+j^2}}\sqrt{\frac{\varepsilon_m\varepsilon_d}{\varepsilon_m+\varepsilon_d}} \tag{3}$$

Therefore, the reflectinction peak (resonance order) can be labeled with integers i and j in the optical spectra and strongly depends on the periodicity as shown in Fig. 2. From this figure it is clear that, by increasing the structural periodicity from 400 to 700 nm, only one resonance mode, either (1,0) or

Table 1 Resonance position, linewidth and reflectinction(1-R) intensity of hybrid plasmonic resonance mode of the grating structure with nanorod height of 25 nm, nanorod diameter of 200 nm, spacer height of 20 nm, film thickness of 100 nm, and refractive index of 1.333 at different structural periodicity

Period (nm)	400	500	600	700	800	900	1000
Peak position (μm)	0.60	0.71	0.63	0.70	0.60	0.65	0.65
Intensity	0.83	0.79	0.62	0.32	0.20	0.18	0.19
Linewidth (nm)	17	8	14	6	30	9	10

(1,1), appeared in the spectrum with up to wavelength of 900 nm. However, by further increasing the structural periodicity from 800 to 1000 nm, two resonance modes with higher resonance orders appeared in the spectrum.

As can be seen from Fig. 2 and Table 1, the resonance intensity of the reflectinction was reduced monotonically by increasing the structural periodicity, and the resonance linewidth varied in the range of 6 to 30 nm. The reduced reflectinction intensity at larger periodicity is due to the smaller duty cycle (the ratio of nanorod diameter and periodicity). For infinite periodicity, the reflection would approach unity for large wavelength as in the case for flat gold film. The minimum and maximum linewidth values were calculated at structural period of 700 and 800 nm as 6 and 30 nm, respectively.

From Table 1, it is also evident that, the structural periodicity of 700 nm possesses the hybrid resonance mode with minimum linewidth value, yet the reflectinction intensity (resonance intensity) was less than 40 %. The optimum structural periodicity which gives simultaneously large hybrid

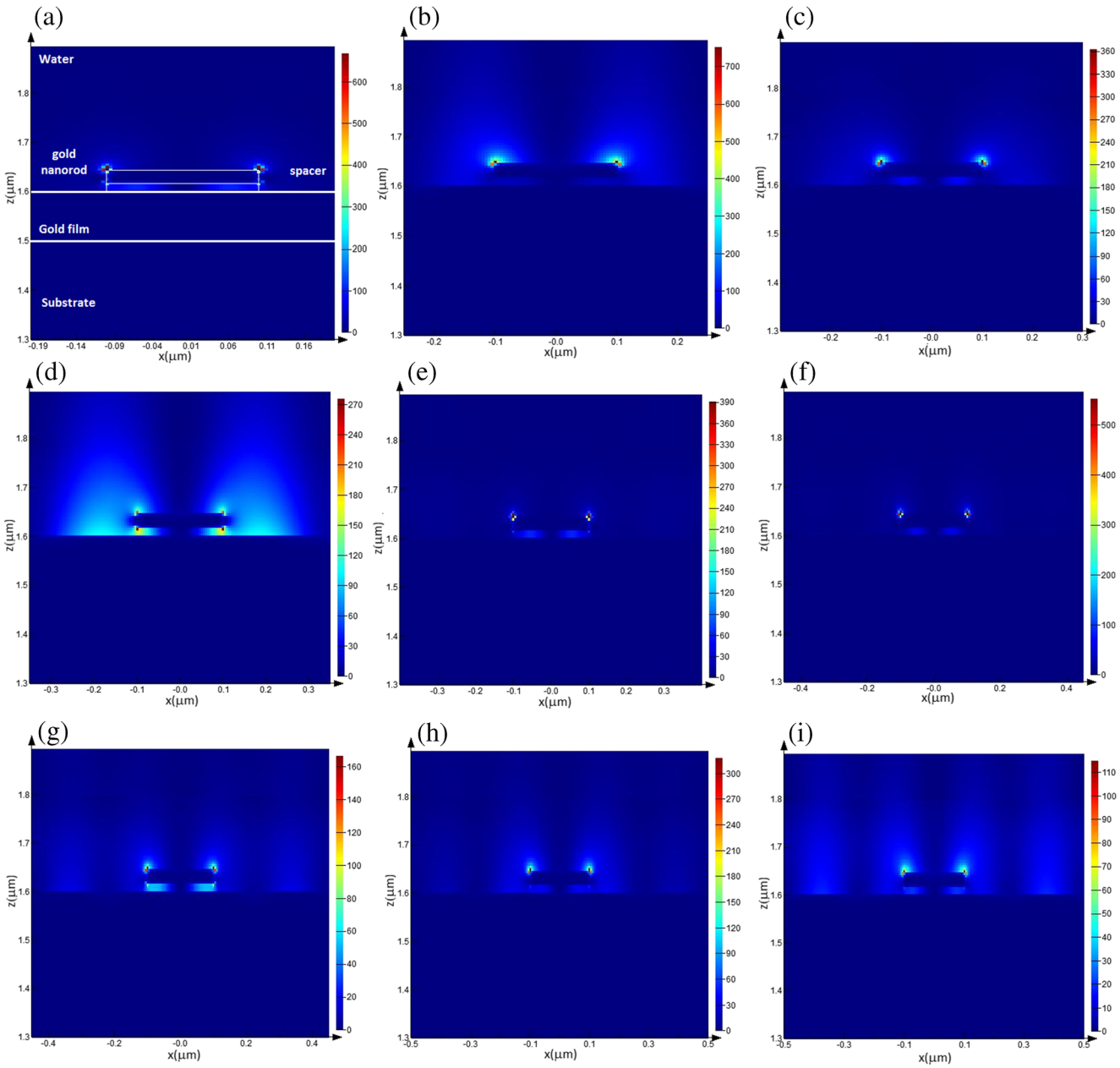

Fig. 3 The electric field profile of the reflectinction resonance modes of the Au-NROM grating structure at **a** P=400 nm, λ=605; **b** P=500 nm, λ=710 nm; **c** P=600 nm, λ=626 nm; **d** P=700 nm, λ=705 nm; **e** P=800 nm, λ=601 nm; **f** P=900 nm, λ=604 nm; **g** P=900 nm, λ=652 nm; **h** P=1000 nm, λ=649 nm; and **i** P=1000 nm, λ=710 nm. The nanorod height, nanorod diameter, spacer height, film thickness, and ambient medium refractive index were fixed at 25 nm, 200 nm, 20 nm, 100 nm, and 1.333, respectively

reflectinction intensity and narrow linewidth value is 500 nm. Therefore, this structural periodicity (i.e., 500 nm) was chosen as optimum period for further analysis.

Figure 3 shows the electric field profile of the hybrid resonance modes of reflection spectra presented in Fig. 2 for different structural periodicity of the Au-NROM grating structures. As it is evident that from this figure, the electric field confinement around the nanorods was reduced by increasing the structural periodicity, which is in agreement with reflectinction spectra data in Fig. 2 and Table 1. As can be seen from this figure, the highest $|E|^2$ was recorded as $753\,(\mathrm{V/m})^2$ in the Au-NROM structure with period of 500 nm (Fig. 3b), whereas the minimum $|\mathrm{E}|^2$ was recorded as $115\ (\mathrm{V/m})^2$ in the grating structure with period of 1000 nm (Fig. 3i) that is related to the (2,1) resonance mode. From Fig. 3c–i, it can be seen that by increasing the structural periodicity, the electric field confinement of the hybrid mode was reduced which leads to lower $|E|^2$ values. It is also found that, in the Au-NROM grating structure with period of 700 nm, more electric field extended into the target liquid (i.e., water in Fig. 3d).

The Effects of Varying Spacer and Nanorod Heights

A series of Au-NROM grating structures with period of 500 nm, film thickness of 100 nm, nanorod diameter of 200 nm, different nanorod heights in the range of 25 to 75 nm, and different spacer heights in the range of 10 to 50 nm were numerically investigated. Figure 4 shows the effects of varying spacer height on reflection resonance wavelength by recording the reflection spectrum at 200 nm above the structure.

As can be seen from Fig. 4, there are not any significant changes in the resonance wavelength position by increasing the spacer height from 10 to 50 nm in Au-NROM with nanorod height in the range of 25 to 75 nm; however, there are significant variations in the resonance wavelength in the Au-NROM structure with smaller nanorod height of 10 and 15 nm. This blue shift in the resonance wavelength could be due to the weaker coupling between the surface plasmon modes at the nanorod/spacer interface and spacer/Au film interface.

This can be explained by considering the electrical effect variation of two thin metallic layers based on the decreased interference effects between the real electric dipole moment (nanorod/spacer interface) and imaginary electric dipole moment (Au film/space interface) with increasing the distance between electric dipoles. As it is clear from Fig. 4, the reflectinction intensity was slightly increased by increasing the spacer height. The resonance mode was observed at wavelength of 711 nm which could be attributed to LSP-SPP resonance hybrid mode [36, 37] as it is also shown in Fig. 5.

From Fig. 4, it is obvious that the linewidth of the hybrid resonance mode at wavelength of 711 nm was reduced by reducing the nanorod height. However, the reflectinction also dropped quickly for small nanorod height. The reflectinction would approach that of a flat Au film for zero nanorod height. A high reflectinction intensity together with a narrow resonance linewidth as small as 7 nm was acquired at nanorod height of 25 nm. Therefore, the nanorod height of 25 nm was considered as optimum height for further analysis.

The magnitude of electric field profiles of the resonance hybrid mode in a grating structure in water with nanorod height of 25 nm, nanorod diameter of 200 nm and film thickness of 100 nm, and different spacer heights in the range of 10

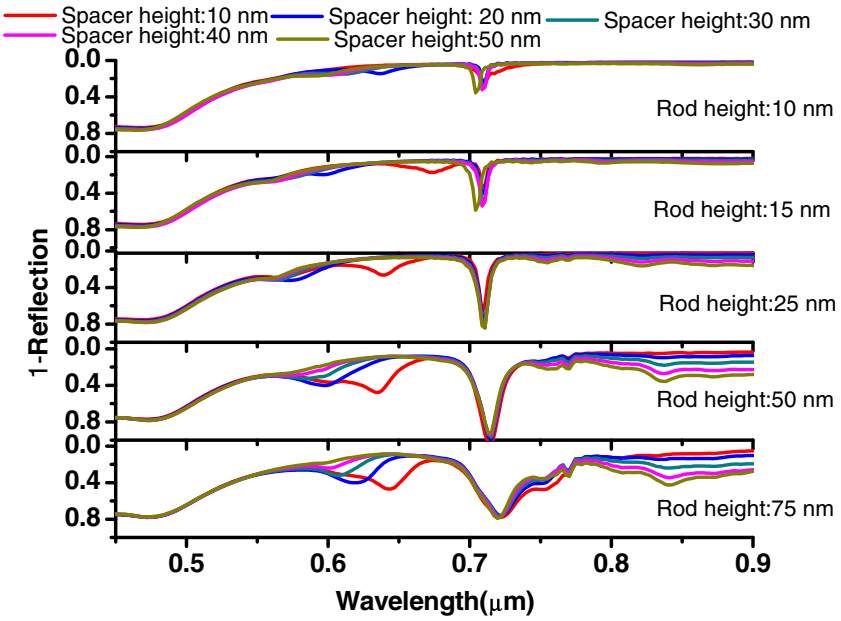

Fig. 4 FDTD reflectinction spectrum of the Au-NROM grating structures at different spacer heights and nanorod heights. The film thickness, structural periodicity, and refractive index of ambient medium were fixed at 100 nm, 500 nm, and 1.333, respectively

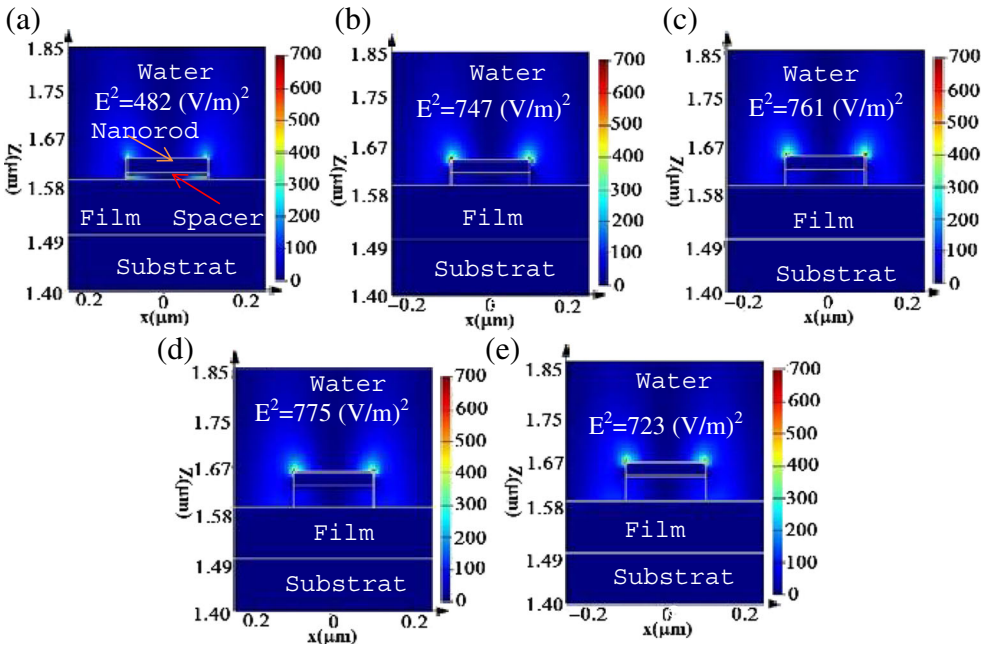

Fig. 5 The electric profile of hybrid mode at wavelength of 711 nm in a grating structure of period of 500 nm, nanorod height of 25 nm, nanorod diameter of 200 nm, film thickness of 100 nm, and spacer height of **a** 10, **b** 20, **c** 30, **d** 40, and **e** 50 nm

to 50 nm is shown in Fig. 5. From this figure, it is clear that by increasing the spacer height from 10 (Fig. 5a) to 50 nm (Fig. 5e), the electric field enhancement increased until it reached its maximum ($|E|^2$=775(V/m)^2) at spacer height of 40 nm (Fig. 5c) and then decreased gradually by increasing the spacer height to 50 nm ($|E|^2$=723(V/m)^2). It is also evident that the LSP resonance mode dominants the SPP for spacer height larger than 20 nm.

This phenomenon could be explained by considering the nature of coupling phenomenon between the two types of surface plasmons. In the Au-NROM structure, the incident light can directly excite the LSP of the nanorods. However, there is not any direct excitation of SPPs due to momentum mismatch between the in-plane wavevector of surface plasmon polaritons, k_{SPP}, and the wavevector component of incident light which is traveling in the water between the film surface and nanorods and dielectric pillars (spacer) [28]. Therefore, excitation of hybrid (LSP-SPP) mode was acquired as a result of coupling between induced surface image of electric dipole in gold film and real one in the nanorod [28].

Figure 6 shows the variation of optical properties of LSP-SPP hybrid mode as a function of spacer height for an Au-NROM structure of nanorod height and nanorod diameter of 25 and 200 nm, respectively. The structural periodicity, film thickness, and liquid refractive index were fixed at 500 nm, 100 nm, and 1.333, respectively. As can be seen from this figure, the minimum linewidth (7 nm) was observed at spacer height of 10 nm, which was accompanied by the reflectinction intensity of 66 %. For a balanced linewidth and reflectinction intensity, we consider the spacer height of 30 nm, which leads to resonance linewidth of 8.4 nm and reflectinction intensity of 82 % as the optimum value for further analysis and sensing application.

Figure 7 shows the resonance peak position, resonance linewidth, and resonance intensity as a function of liquid refractive index of the Au-NROM structures with spacer height in range of 10 to 50 nm and nanorod height of 25 nm. The structural periodicity, film thickness and nanorod diameter were fixed at 500, 100, and 200 nm, respectively. As can be seen from Fig. 7a, the resonance wavelength position was shifted toward larger wavelength by increasing the liquid refractive index and reached 733 nm at 1.377. It was also found

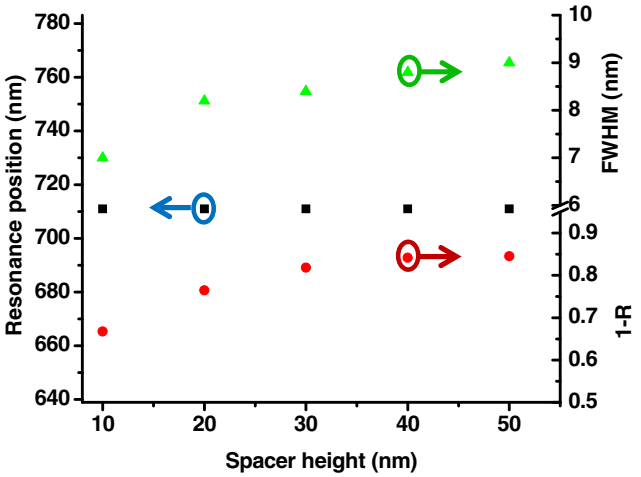

Fig. 6 Resonance position, reflectinction intensity (1-R), and linewidth of hybrid mode in an Au-NROM structure as a function of spacer height. The nanorod height, nanorod diameter, film thickness, structural period, and liquid refractive index were fixed at 25 nm, 200 nm, 100 nm, 500 nm, and 1.333, respectively

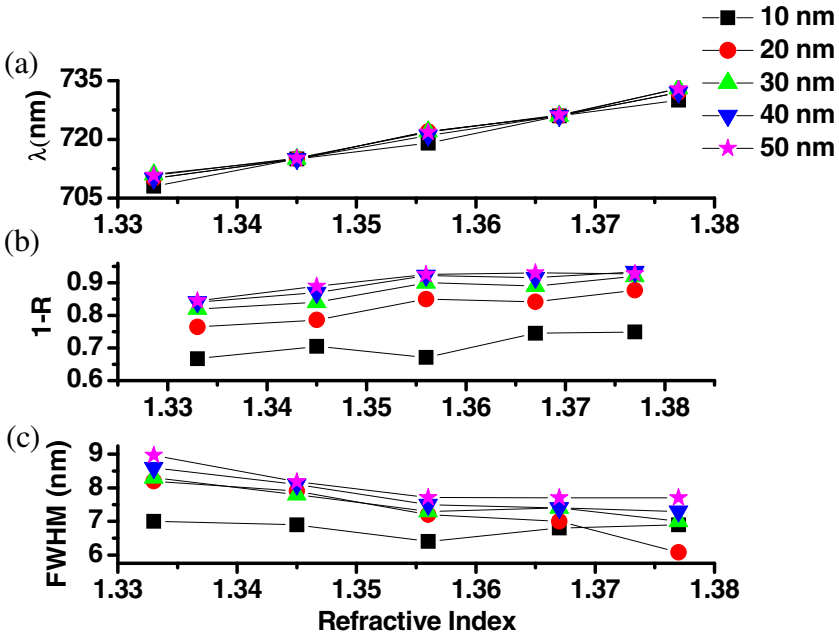

Fig. 7 **a** Resonance position, **b** reflectinction intensity (1-R), and **c** linewidth of a grating structure with spacer height of 10 nm (—■—), 20 nm (—●—), 30 nm (—▲—), 40 nm (—▼—), and 50 nm (—★—), as a function of liquid refractive index. The structural periodicity, film thickness, nanorod height, and nanorod diameter were fixed as 500, 100, 25, and 200 nm, respectively

that the resonance wavelength position was increased linearly by increasing the refractive index.

From Fig. 7b, it is evident that the reflectinction resonance intensity was increased gradually by increasing both refractive index and spacer height. For example, in the Au-NROM structure with spacer height of 50 nm, the resonance peak intensity was increased from 84 to 93 % by increasing the refractive index from 1.333 to 1.377. The effects of spacer height variations on the resonance linewidth of grating structure were compared in Fig. 7c. It is clear that by increasing the refractive index, the linewidth of the resonance hybrid mode was reduced slowly, and a maximum reduction of 2.6 nm were observed in a grating structure with spacer height of 20 nm. This reduction could be due to lower dispersive properties of Au at higher resonance wavelength for larger refractive index which leads to smaller resonance linewidth of SPP and therefore increased coupling strength between the LSP resonance mode and SPP resonance mode. The maximum and minimum linewidth values were calculated as 8.3 nm (at n=1.333) and 7 nm (at n=1.377), respectively.

Surface Sensing

The effects of using liquids with different refractive indices in the range of 1.333 to 1.377 on the sensing properties of the designed Au-NROM grating structure were studied numerically. The surface of the Au-NROM grating structure was covered by water (n=1.333), trimethylamine (n=1.345), acetone (n=1.356), human hemoglobin (n=1.367), and IPA (n=1.377). The effects of variation of spacer height on the sensitivity ($\Delta\lambda/\Delta n$) and figure of merit (FOM=Sensitivity/linewidth) of the Au-NROM structure are detailed in Table 2.

It was found that by increasing the spacer height from 10 to 50 nm, the sensitivity and FOM were reduced generally. The sensitivity of the Au-NROM grating structure at larger refractive index (n=1.377) was calculated as 500 nm/RIU for all spacer heights in the range of 10 to 50 nm. It can also be seen that the sensitivity and FOM values of the Au-NROM structure with spacer height of 30 nm was increased linearly by increasing the refractive index of the target liquid.

Figure 8 shows the FDTD simulated reflection spectrum of the Au-NROM of spacer height of 30 nm, nanorod height of 25 nm, and different refractive indices. As can be seen from this figure, the resonance reflection peaks were varied in the range of 711 to 733 nm.

From Fig. 8a, it can be seen that by increasing the refractive index, the resonance wavelength was increased by 22 nm and

Table 2 Sensitivity and FOM of the grating structure for sensing different liquids relative to water (n=1.333), with nanorod height of 25 nm, nanorod diameter of 200 nm, film thickness of 100 nm and structural periodicity of 500 nm, and different spacer heights in the range of 10 nm to 50 nm

Spacer height (nm)	Sensitivity (nm/RIU)				FOM (RIU^{-1})			
	Δn				Δn			
	0.012	0.023	0.034	0.044	0.012	0.023	0.034	0.044
10	584	478	529	500	83	67	78	74
20	417	522	470	500	52	73	66	74
30	333	478	470	500	51	63	63	68
40	417	478	441	500	40	67	59	71
50	333	478	441	500	41	59	57	65

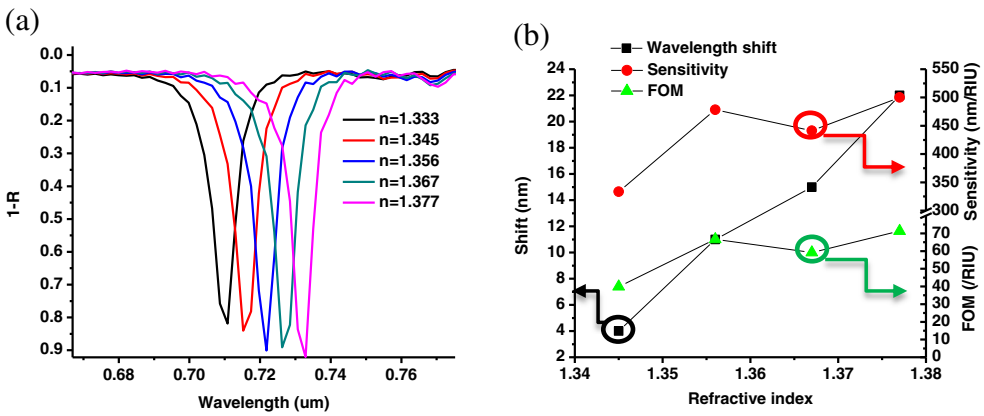

Fig. 8 **a** FDTD reflectinction spectrum and **b** wavelength shift (relative to n=1.333), FOM (figure of merit = sensitivity/linewidth) and sensitivity ($\Delta\lambda/n$(=1.333)) of the Au-NROM structure covered with liquids with different refractive indices. The film thickness, nanorod diameter, nanorod height, spacer height, and structural periodicity were fixed at 100, 200, 25, 30, and 500 nm, respectively

the resonance linewidth was reduced by 1.3 nm. The maximum and minimum linewidth of 8.3 and 7.0 nm, respectively, were calculated for water and IPA as sensing liquids. From Fig. 8b, it is clear that the sensitivity of the Au-NROM with spacer height of 30 nm was larger for larger refractive index change, and the maximum sensitivity was acquired as 500 nm/RIU at Δn=0.044 (=1.377–1.333). It can be concluded that this grating structure could be a promising candidate for sensing liquids (whose refractive index is close to the water) with respect to high purity water. This includes salinity and human hemoglobin concentration measurement using visible light source [38].

Conclusion

The reflection resonance wavelength, resonance linewidth, and sensitivity of the Au-NROM grating structure were investigated. It was shown that the grating structure was performed larger sensitivity for larger refractive indices. An acceptable FOM value in the range of 40 to 71 was obtained in an Au-NROM structure using high purity water as reference, which promising new reflection based sensor for sensing liquids with close refractive index to the water in the visible range such as human hemoglobin and salinity sensors. The narrow resonance linewidth as small as 7 nm was obtained at maximum sensitivity of 500 nm/RIU at refractive index change of 0.044 for reflection spectrum in an Au-NROM grating structure with optimum geometrical parameters. While, the minimum linewidth of 10 nm was reported by Cetin et al. [24] using Fano resonance and SPP mode coupling and transmission spectrum. The minimum sensitivity was obtained as 333 nm/RIU at refractive index of 0.012 (Δn=1.345–1.333). Moreover, the reflectinction intensity of the Au-NROM grating structures was changes slightly by increasing the spacer height. It was also shown that the due to excitation of image surface electric dipole in the gold film (mirror), the LSP-SPP coupling was more dominant than only the LSP resonance mode [12].

References

1. Coe JV et al (2008) Extraordinary transmission of metal films with arrays of subwavelength holes. Annu Rev Phys Chem 59(1):179–202
2. García de Abajo FJ (2007) Colloquium: light scattering by particle and hole arrays. Rev Mod Phys 79(4):1267–1290
3. Garcia-Vidal FJ et al (2010) Light passing through subwavelength apertures. Rev Mod Phys 82(1):729–787
4. Guo J, Adato R (2006) Extended long range plasmon waves in finite thickness metal film and layered dielectric materials. Opt Express 14(25):12409–12418
5. Hess O et al (2012) Active nanoplasmonic metamaterials. Nat Mater 11(7):573–584
6. Tang ZH et al (2007) Coupling of surface plasmons in nanostructured metal/dielectric multilayers with subwavelength hole arrays. Phys Rev B 76(19):195405
7. Vial A, Laroche T (2007) Description of dispersion properties of metals by means of the critical points model and application to the study of resonant structures using the FDTD method. J Phys D Appl Phys 40:7152–7158
8. Xiao S, Mortensen NA, Qiu M (2007) Enhanced transmission through arrays of subwavelength holes in gold films coated by a finite dielectric layer. J Eur Opt Soc-Rapid 2:07009
9. Lal S, Link S, Halas NJ (2007) Nano-optics from sensing to waveguiding. Nat Photonics 1(11):641–648
10. Atwater HA, Polman A (2010) Plasmonics for improved photovoltaic devices. Nat Mater 9(3):205–213
11. Luk'yanchuk B et al (2010) The Fano resonance in plasmonic nanostructures and metamaterials. Nat Mater 9(9):707–715
12. Mubeen S et al (2012) Plasmonic properties of gold nanoparticles separated from a gold mirror by an ultrathin oxide. Nano Lett 12(4):2088–2094
13. Roh S, Chung T, Lee B (2011) Overview of the characteristics of micro- and nano-structured surface plasmon resonance sensors. Sensors 11(2):1565–1588
14. Chiu N-F, Tu Y-C, Huang T-Y (2013) Enhanced sensitivity of anti-symmetrically structured surface plasmon resonance sensors with zinc oxide intermediate layers. Sensors 14(1):170–187
15. Galush WJ et al (2009) A nanocube plasmonic sensor for molecular binding on membrane surfaces. Nano Lett 9(5):2077–2082

16. Jain PK, El-Sayed MA (2008) Noble metal nanoparticle pairs: effect of medium for enhanced nanosensing. Nano Lett 8(12):4347–4352
17. Maier SA (2007) Plasmonics: fundamentals and applications. Springer, New York
18. Hutter E, Fendler JH (2004) Exploitation of localized surface plasmon resonance. Adv Mater 16(19):1685–1706
19. Tian XR, Tong LM, Xu HX (2013) New progress of plasmonics in complex metal nanostructures. Sci China Phys Mech Astron 56(12): 2327–2336
20. Mayer KM, Hafner JH (2011) Localized surface plasmon resonance sensors. Chem Rev 111(6):3828–3857
21. Anker JN et al (2008) Biosensing with plasmonic nanosensors. Nat Mater 7(6):442–453
22. Irannejad M, Cui B (2013) Effects of refractive index variations on the optical transmittance spectral properties of the nano-hole arrays. Plasmonics 8(2):1245–1251
23. Kim D (2006) Effect of resonant localized plasmon coupling on the sensitivity enhancement of nanowire-based surface plasmon resonance biosensors. J Opt Soc Am A 23(9):2307–2314
24. Cetin AE, Altug H (2012) Fano resonant ring/disk plasmonic nanocavities on conducting substrates for advanced biosensing. ACS Nano 6(11):9989–9995
25. Hentschel M et al (2010) Transition from isolated to collective modes in plasmonic oligomers. Nano Lett 10(7):2721–2726
26. Davis TJ, Gómez DE, Vernon KC (2010) Simple model for the hybridization of surface plasmon resonances in metallic nanoparticles. Nano Lett 10(7):2618–2625
27. Jian Y et al (2009) Observation of plasmonic dipolar anti-bonding mode in silver nanoring structures. Nanotechnology 20(46):465203
28. Mock JJ et al (2008) Distance-dependent plasmon resonant coupling between a gold nanoparticle and gold film. Nano Lett 8(8):2245–2252
29. Jackson JD (1999) Classical electrodynamics. John Wiley & Sons, New York
30. Lumdee C, Yun B, Kik PG (2013) Wide-band spectral control of au nanoparticle plasmon resonances on a thermally and chemically robust sensing platform. J Phys Chem C 117(37):19127–19133
31. Sullivan DM (2000) Electromagnetic simulation using the FDTD method. IEEE Press Series, New York
32. Rakic AD et al (1998) Optical properties of metallic films for vertical-cavity optoelectronic devices. Appl Opt 37(22):5271–5283
33. Alexandre V, Thierry L (2007) Description of dispersion properties of metals by means of the critical points model and application to the study of resonant structures using the FDTD method. J Phys D Appl Phys 40(22):7152
34. Available from: http://docs.lumerical.com/en/fdtd/user_guide_symmetric_anti_symmetric.html
35. Ghaemi HF et al (1998) Surface plasmons enhance optical transmission through subwavelength holes. Phys Rev B 58(11):6779–6782
36. Wu D, Liu X (2010) Optimization of the bimetallic gold and silver alloy nanoshell for biomedical applications in vivo. Appl Phys Lett 97(6):-
37. Yun-Chorng C et al (2013) A large-scale sub-100 nm Au nanodisk array fabricated using nanospherical-lens lithography: a low-cost localized surface plasmon resonance sensor. Nanotechnology 24(9): 095302
38. Zhernovaya O et al (2011) The refractive index of human hemoglobin in the visible range. Phys Med Biol 56(13):4013